

Mixture Fraction Analysis of Combustion Products in Medium-Scale Pool Fires

Ryan Falkenstein-Smith*, Kunhyuk Sung, Anthony Hamins

National Institute of Standards and Technology, 100 Bureau Dr., Gaithersburg, MD 20899, United States of America

Abstract

A mixture fraction analysis is performed to investigate the characteristics of time-averaged gaseous species measurements made along the centerline of medium-scale pool fires steadily burning in a quiescent environment. A series of fire experiments are conducted using 30 cm diameter liquid and 37 cm diameter gas pool burners. All gaseous species measurements are extracted at various heights within the fire and analyzed using an Agilent 5977E Series Gas Chromatograph with mass selectivity and thermal conductivity detectors. Soot mass fractions are simultaneously measured during gas sampling. For all fuels, the results show that the local composition plotted as a function of mixture fraction collapses the experimental data into a few coherent lines that nearly match the idealized reactions. Differences between the theoretical and experimental data are attributed to the presence of carbon monoxide, soot, and other intermediate carbon-containing species. The ratio of carbon monoxide and soot is presented as a function of mixture fraction in which a trend is observed.

Keywords:

Mixture fraction, Pool fires, Carbon-to-Hydrogen ratio, Combustion products, Chemical composition

*Corresponding author: Ryan Falkenstein-Smith

Email address: ryan.falkenstein-smith@nist.gov (Ryan Falkenstein-Smith)

1. Introduction

Computational fluid dynamics (CFD) models are an important component of performance-based design in fire protection engineering. A requirement of their acceptance in the design process is that these models be verified and validated, the latter of which involves comparison with experimental measurements. The primary objective of this work is to provide data for use in fire model validation.

Mixture fraction-based combustion analysis has been widely used to characterize combustion chemistry of different fires [1–5], which is essential when improving the accuracy of fire model predictions. A mixture fraction-based combustion model assumes that the combustion is mixing-controlled, and the reaction between fuel and oxygen is taking place on an infinitely thin flame sheet. This assumption is well-suited for over-ventilated conditions such as pool fires.

In a pool fire, the fuel surface is isothermal, flat, and horizontal, providing a well-defined boundary condition for modeling. Fuel and product species concentrations and temperatures have a significant influence on the heat feedback to the fuel surface, which directly affects the burning rate. A zone of particular interest is the fuel-rich core between the flame and the pool surface, where gaseous species can absorb radiation that would otherwise have been transferred to the fuel surface. Few studies in the literature have reported local chemical species measurements within the flame envelope.

In this study, a mixture fraction analysis is performed to characterize the spatial distribution of the principal chemical species in moderate-scale pool fires steadily burning in a well-ventilated, quiescent environment. A series of fire experiments is conducted using a 30 cm diameter liquid and 37 cm diameter gas pool burner. Gaseous species and soot measurements are made at various heights within the fire. Four fuels are considered: methane, methanol, ethanol, and acetone. Through the analysis of the species composition at various locations within the fire, this study attempts to provide insight into the combustion chemistry of pool fires.

2. Description of Experiments

2.1. Pool Burner Setup

All experiments are conducted under a canopy hood surrounded by a cubic enclosure, 2.5 m on a side, made of a double layer wire-mesh screen (5 mesh/cm) to reduce the impact of room ventilation. All measurements

are made once the mass burning rate reaches a steady-state, achieved approximately 10 min and 2 min after ignition for the liquid and methane fuels, respectively.

Liquid fuels are burned in a circular, stainless-steel pan, made from cold-rolled steel, with a diameter of 30.1 cm, a depth of 15 cm, and a wall thickness of 1.3 mm. The liquid burner has an overflow basin, which extends 2.5 cm beyond the burner wall. Fuel to the liquid burner is gravity fed from a reservoir positioned on a mass load cell located outside the enclosure and is manually controlled by adjusting the fuel flow using a needle valve. The fuel surface is maintained 10 mm below the burner rim to match previous experimental conditions [6–9]. Methane is burned using a 37 cm diameter burner. Fuel to the gas burner is controlled via a mass flow controller located outside of the enclosure. The bottoms of both burners are maintained at a constant temperature by flowing water ($20\text{ }^{\circ}\text{C} \pm 3\text{ }^{\circ}\text{C}$). Further descriptions of the liquid and gas burners are found in Refs. [7, 10–14].

The mean flame height is estimated from 3600 frames of high-resolution video of the experiments using MATLAB's Image Processing Toolbox¹. Imported color images are decomposed into binary (i.e., black and white) images using a pre-set threshold level. The flame height for a single frame is defined as the distance between the pool surface and flame tip. All measurements are repeated, then averaged to provide the mean flame height.

2.2. Measuring the Volume Fraction of Gaseous Species

Gaseous species measurements are made using an Agilent 5977E Series Gas Chromatograph with mass selectivity and thermal conductivity detectors (GC/MSD). Figure 1 displays the flow diagram for gas sampling. The gases are extracted by a vacuum pump located downstream of the GC/MSD. Gas samples are collected using a quenching probe, which is composed of two concentric, stainless-steel tubes with outer annular coolant flow and inner, extracted sample flow. The inner and outer tube diameters are 8 mm and 16 mm, respectively. Water at approximately $90\text{ }^{\circ}\text{C}$ flows through the sampling probe during sampling. The remainder of the sampling line leading into the GC/MSD is heated with electrical heating tape to approximately $140\text{ }^{\circ}\text{C}$ to prevent condensation of water and liquid fuels within the line.

¹ Certain commercial products are identified in this report to specify adequately the equipment used. Such identification does not imply a recommendation by the National Institute of Standards and Technology, nor does it imply that this equipment is the best available for the purpose.

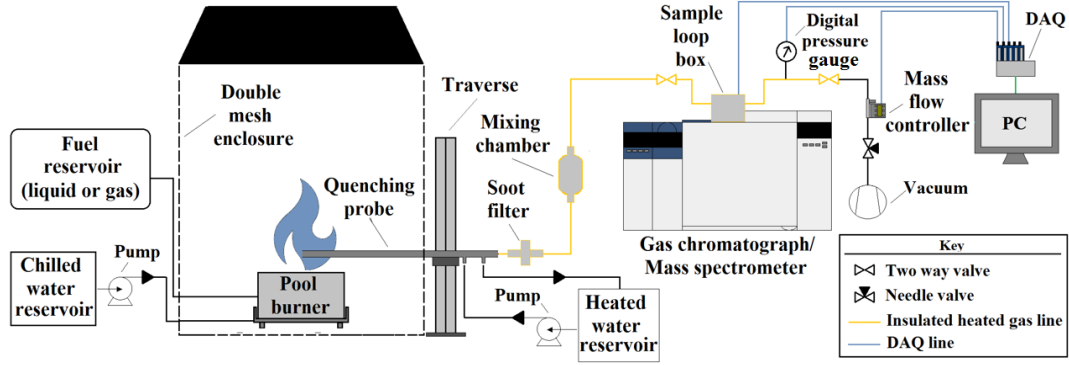


Figure 1: A schematic of the extraction sampling and analysis system.

Depending on the probe location within the fire, the sampling period varies from 12 min to 25 min, ensuring a sufficient mass of soot and gas sample is collected. The flow is controlled using a mass flow controller (Alicat Scientific MC-Series) located in front of the vacuum pump within the sampling line. During the gas sampling procedure, the volumetric flow is approximately 200 mL/min and recorded at 2 Hz. All measurements using the GC/MSD are repeated at least twice at each location along the centerline of the pool fire. Gaseous species concentration measurements made at the same location are averaged. The mean mass fraction, \bar{Y}_i , of a given species i is calculated from the measured volume fraction, \bar{X}_i , using the following expression:

$$\bar{Y}_i = \frac{\bar{X}_i W_i}{\sum \bar{X}_i W_i} \quad (1)$$

where W_i is the molecular weight of a given species.

2.3. Centerline Temperature Measurements

Time-averaged temperature measurements are made along the centerline profiles of the pool fires at the same gas sampling locations. An S-type (Pt 10% Rh/Pt), bare-wire, thermocouple (OMEGA P10R-001) with a 50 μm wire diameter and a bead diameter of approximately 150 μm is used. Temperature measurements are sampled at 250 Hz for 2 min, or approximately 300 pulsing cycles [15]. The thermal inertia and radiative heat loss associated with the thermocouple are corrected following the method of Shaddix [16].

2.4. Determining Soot Mass Fraction

Soot mass fraction, Y_s , is measured using a well-established gravimetric technique [17]. Soot is filtered out of the gas stream using a stainless steel particulate filter holder (PALL 2220). Before an experiment, a desiccated 47 mm polytetrafluoroethylene (PTFE) filter is

weighed and placed into its holder. The filter holder is positioned within the gas sampling line behind the quenching probe and heated with tape to approximately 140 $^{\circ}\text{C}$ to prevent condensation of water and liquid fuels on the filter. After sampling, the filter is removed and dried in a desiccator. After drying for 48 h, the filter's final weight is measured. Approximately 1 mg of soot is collected during the sampling period. The mass of the PTFE filter and cleaning patches are measured three times before and after each test. After most experiments, soot deposits are observed on the inner walls of the quenching probe. Dedicated gun cleaning patches (Hoppe's 9 1203S) are used to clean the inside of the quenching probe with no cleaning solvent. At least two patches are used to collect soot on the inside of the probe. A petri dish is placed below one end of the probe to catch dislodged soot and patches. Soot collection on the inside of the probe concludes once an applied patch is observed to have no soot. Patches are weighed immediately before and 48 h after cleaning the inside of the probe.

The soot mass fraction, Y_s , is computed from the mass of the soot collected from the PTFE filter and gun cleaning patches, m_s , the ratio of the mass flow controller's temperature reading, T_{∞} , to the effective temperature of the gas obtained from the thermocouple measurements, T_g , the total mass of gas sampled, m_{tot} , based on the mass flow controller readings:

$$Y_s = \frac{m_s V_s}{\bar{V} \Delta t m_{\text{tot}}} \frac{T_{\infty}}{T_g} \quad (2)$$

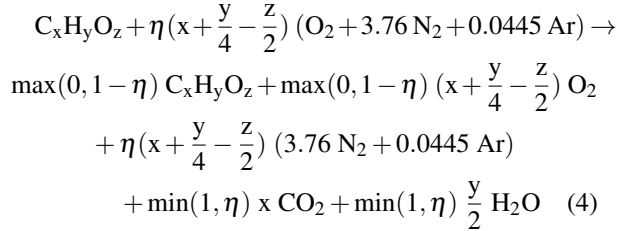
where the total mass of gas sampled is represented by the product of the average volumetric flow rate measured by the mass flow controller, \bar{V} , the gas sampling time, Δt and the gas density. The gas density is represented by the ratio of total mass detected from the GC/MSD, m_{tot} and the injected sample volume, V_s .

2.5. Mixture Fraction Calculation

The mixture calculation follows the same approach as Ref. [18]. The mixture fraction, Z , is defined as the mass fraction of the gases containing carbon, including to soot, that originate in the fuel stream. It can be expressed as follows:

$$Z = \bar{Y}_F + \frac{W_F}{x} \sum_{i \neq F} \frac{\bar{Y}_i}{W_i} \quad (3)$$

where \bar{Y}_F , W_F , and x are the mass fraction, molecular weight, and number of carbon atoms in the fuel molecule, respectively. Assuming ideal (i.e. no CO or soot), infinitely-fast (fuel and oxygen from the air cannot co-exist) combustion, the mass fractions of all species can be expressed as piece-wise linear “state relations” according to the following reaction:



The parameter η is the reciprocal of the local fuel equivalence ratio, ϕ ,

$$\phi = \frac{(F/A)}{(F/A)_{st}} = \frac{1}{\eta} \quad (5)$$

where F/A is the fuel-air mass ratio and the subscript st denotes the stoichiometric condition. The idealized mass fractions of the products are obtained from the right side of Eq. 4. The stoichiometric mixture fraction, Z_{st} , using the following expression:

$$Z_{st} = \frac{W_F}{W_F + W_A} \quad (6)$$

The calculated stoichiometric mixture fractions for the fuels investigated in this work are presented in Table 1.

2.6. Uncertainty Analysis

An extensive uncertainty analysis of measurements is provided in Ref. [19]. The variance between repeated measurements is the most significant contributor to the uncertainties. The uncertainties are expressed using a 95% confidence level. The uncertainty of the mixture fraction is a function of the uncertainties in the carbon carrying species:

$$u_Z^2 = u_{\bar{Y}_F}^2 + \left(\frac{W_F}{x} \right)^2 \sum_{i \neq F} \left(\frac{u_{\bar{Y}_i}}{W_i} \right)^2 \quad (7)$$

Table 1: List of measurements and thermochemical properties of fuels burning in well-ventilated round pool fires

Parameter (units)	Methanol	Ethanol	Acetone	Methane
Diameter (cm)	30.1	30.1	30.1	37.0
Mass Burning Flux (g/m ² s)	12.4 ± 1.1	13.9 ± 0.8	17.6 ± 2.7	6.4 ± 0.1
Heat Release Rate (kW)	17.4 ± 1.4	26.3 ± 1.5	35.5 ± 5.4	34.5 ± 0.5
Mean Flame Height (cm)	36 ± 16	61 ± 28	91 ± 34	64 ± 31
Z_{st}	0.13	0.10	0.09	0.05
Carbon/Hydrogen Ratio	1/4	1/3	1/2	1/4

where u_Z is the combined uncertainty of the mixture fraction determined from the combined uncertainty of the mass fractions of all carbon carrying species.

3. Results

3.1. Flame Observations

The methanol fire is purely blue, whereas the ethanol, acetone, and methane fires are more luminous and yellow. The measured time-averaged burning rates and calculated heat release rates are listed in Table 1. The heat release rates are calculated from the product of the mass burning flux and the idealized heat of combustion. The methanol fire has the lowest average flame height, followed by the ethanol, methane, and acetone. The measured mean flame heights match Heskestad’s correlation [20] to within measurement uncertainty. The measured flame heights are also within the uncertainty bounds of measurements made by Kim et al. [8].

3.2. Comparison of Fire Structure

Figure 2 displays the time-averaged gas temperatures as a function of mixture fraction. The maximum mean temperature for each fuel peaks is close to their respective stoichiometric mixture fraction values. Methane has the highest peak mean temperature of 1350 K with methanol, ethanol, and acetone exhibiting maximum mean temperatures of 1316 K, 1281 K, and 1190 K, respectively. The methanol temperature profile is in agreement with previous works [15].

Figure 3 shows the soot mass fraction as a function of mixture fraction for the methane, ethanol, and acetone pool fires. No soot is detected in the methanol fire. Acetone’s soot mass fraction peaks in fuel-rich conditions whereas methane and ethanol peak close to stoichiometric conditions. In comparison, the acetone pool fire has a factor of 5 and 6 larger soot mass fraction than ethanol and methane, respectively.

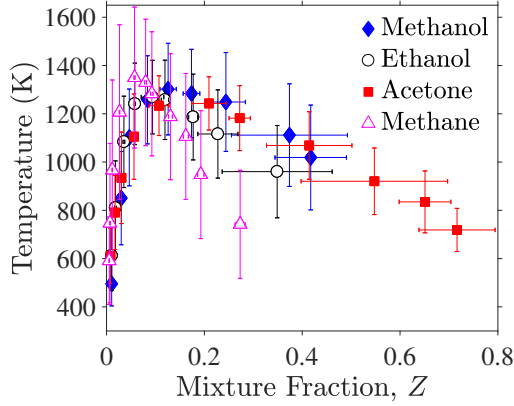


Figure 2: Mean and RMS centerline temperature profiles of methanol, ethanol, acetone, and methane pool fires during their pulsing cycles

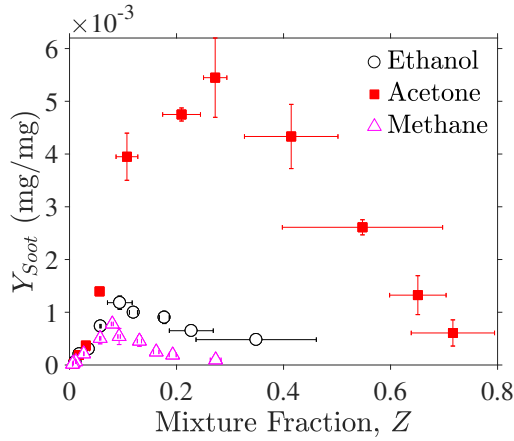


Figure 3: Soot profiles of ethanol, acetone, and methane pool fires

3.3. Verifying Gas Species Measurements

Major species detected in the TCD and MS include combustion reactants (fuels and oxygen, O_2), combustion products such as water, H_2O , and carbon dioxide, CO_2 , combustion intermediates such as carbon monoxide, CO , hydrogen, H_2 , and inert gases such as nitrogen, N_2 , and argon, Ar . Methane is detected and quantified in all fires. In the case of the ethanol, acetone, and methane pool fires, soot, benzene, acetylene, ethylene, and ethane are also detected. As a way to verify the accuracy of the experimental method, the ratio of carbon to hydrogen atoms contained in all gaseous species is calculated at each vertical measurement location using the following function:

$$\frac{C}{H} = \frac{\sum x_i \bar{X}_i}{\sum y_i \bar{X}_i} \quad (8)$$

where the summation is over all measured gaseous species, and x_i and y_i are the numbers of carbon and hydrogen atoms in the molecule, respectively. The carbon-to-hydrogen ratio of the parent fuel molecules are reported in Table 1. As seen in Fig. 4, the theoretical carbon-to-hydrogen ratio for each fuel, represented by the dotted lines, shows agreement with the gaseous species measurements within measurement uncertainty.

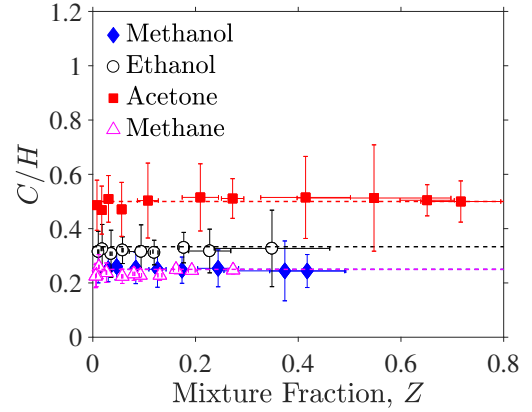


Figure 4: Carbon-to-hydrogen ratio calculated from all measured gaseous species compared to the theoretical values.

3.4. Mixture Fraction Analysis

Figure 5 shows the mean mass fraction measurements as a function of the mixture fraction for the methanol, ethanol, acetone, and methane pool fires, respectively. The combined expanded uncertainty of each measurement is also presented. The dotted lines represent ideal combustion from Eq. (4).

The stoichiometric conditions (see Table 1) can be seen near the intersection of fuel and oxygen at $Y_i = 0$. Where the mixture fraction is much less than stoichiometric, all major gaseous species are in close agreement with the ideal state relations; the measured mass fractions of unburned fuel and CO are nearly zero, and the O_2 is close to its respective theoretical value. The measured mass fraction of CO_2 and H_2O are found to peak close to the stoichiometric mixture fraction. As the mixture fraction increases, the mass fraction of O_2 is nearly zero, whereas the mass fraction of each fuel increases linearly. In the fuel-rich region, the measured mass fraction of CO_2 differs considerably from the ideal state relation due to the substantial amount of CO and soot. This has been observed in other mixture fraction analyses and is attributed to finite rate chemistry effects associated with slow CO chemistry [5]. For the cases of the

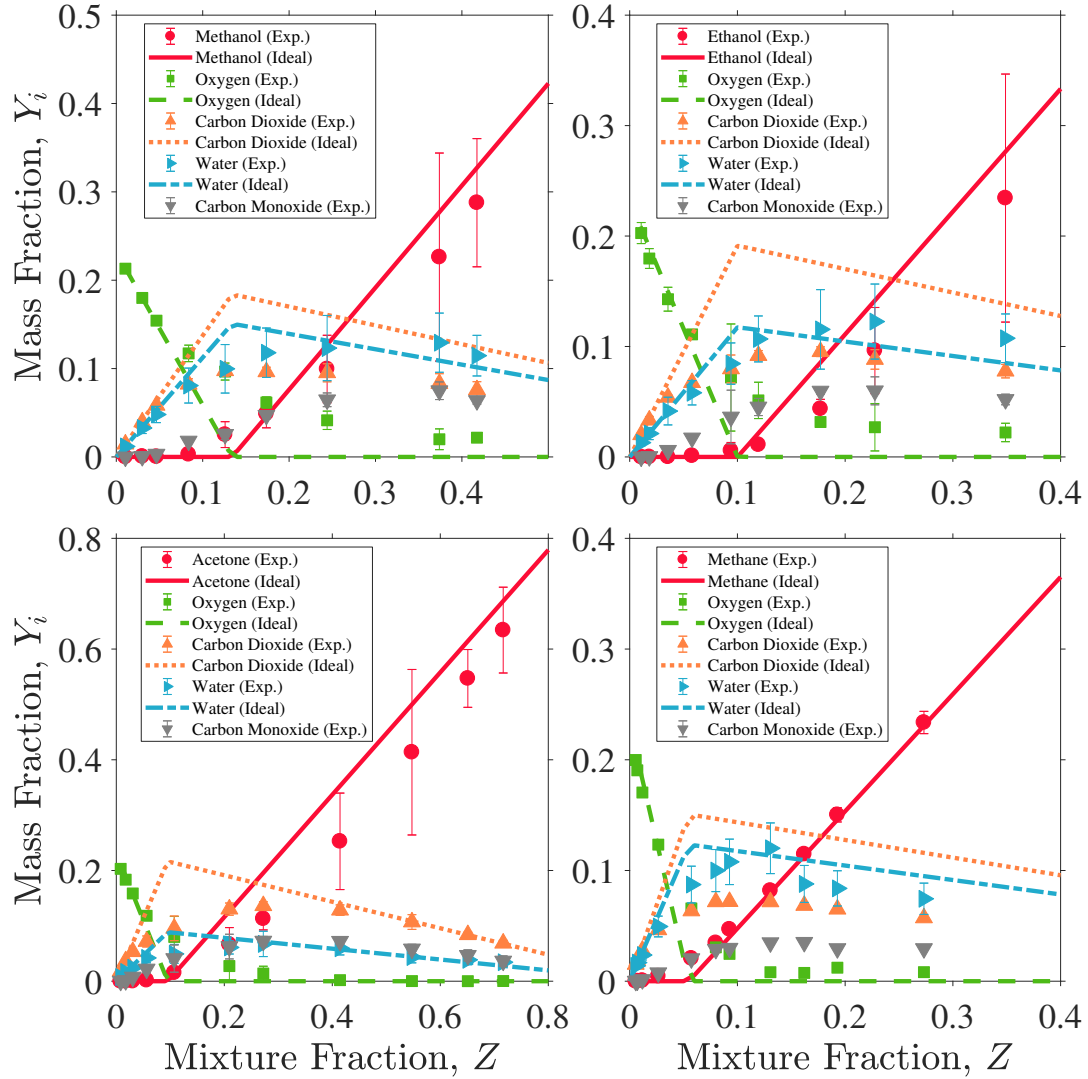


Figure 5: Mean mass fractions as a function of mixture fraction for methanol (top left), ethanol (top right), acetone (bottom left), and methane (bottom right) pool fires.

liquid pool fires, the over-shoot of fuel is likely linked to the presence of other intermediate carbon-containing species close to the fuel surface. This is exemplified in the fuel-rich region for acetone in which the fuel concentration is low while CO_2 is in fair agreement with the state relations; the larger portion of CO and soot, relative to other fuels, could account for the difference.

3.5. Carbon Balance

The measurements show that the elemental carbon was primarily partitioned among CO_2 , CO, CH_4 , and soot. Other hydrocarbons, such as benzene, acetylene, ethylene, and ethane, were measured in trace/small

quantities compared to CH_4 . Figure 6 shows the mass ratio of CO to soot as a function of mixture fraction for the methane, ethanol, and acetone fires. The general trend of each fuel shows that the ratio of CO to soot exponentially decreases as the mixture fraction approaches fuel lean conditions. Köylü et al. [21] reported that the mass-based ratio of CO to soot generation factors in the overfire (i.e., the fuel-lean exhaust stream) region of non-premixed hydrocarbon flames for a range of strongly sooting fuels was 0.34 ± 0.09 . It is observed that the ratio of CO and soot tends to Köylü's value under fuel-lean conditions. However, the measurements made in this work are made within the fire, primarily

below the flame tip, using weakly and non-sooting fuels that do not necessarily match the heavily sooting fuels used by Köylü.

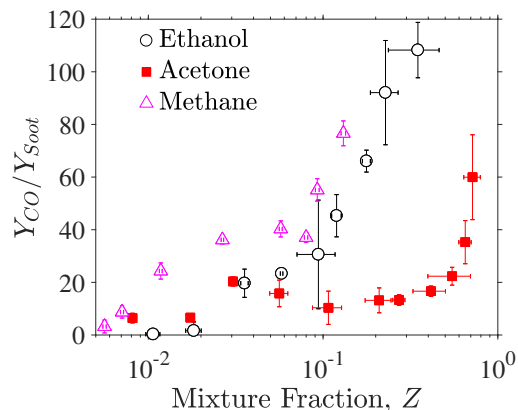


Figure 6: Carbon to soot ratio as a function of mixture fraction.

4. Conclusion

This study characterizes the structure of several medium-scale pool fires steadily burning in a quiescent environment. Temperature and soot centerline profiles for methanol, ethanol, acetone, and methane are reported. The calculated carbon-to-hydrogen ratio at each location is shown to be in agreement with the parent fuel values, which validates the accuracy of the measurements. Major species detected in the centerline profile of the pool fires are represented as a function of mixture fraction. As expected, carbon-containing species are shown to be less than the state relations in fuel-rich regions due to the presence of CO and soot. For methane, ethanol, and acetone fires, the ratio of CO to soot is observed to decline when changing from fuel-rich to fuel-lean conditions.

References

- [1] R. Bilger, Reaction rates in diffusion flames, *Combustion and Flame* 30 (1977) 277–284.
- [2] N. Peters, Laminar diffusion flamelet models in non-premixed turbulent combustion, *Progress in Energy and Combustion Science* 10 (3) (1984) 319–339.
- [3] J. Floyd, C. Wiczkorek, U. Vandsburger, Simulations of the virginia tech fire research laboratory using large eddy simulation with mixture fraction chemistry and finite volume radiative heat transfer, in: *Proceedings of the Ninth International Interflam Conference*. Interscience Communications, London, Vol. 12, 2001.
- [4] A. Hamins, K. Seshadri, The structure of diffusion flames burning pure, binary, and ternary solutions of methanol, heptane, and toluene, *Combustion and Flame* 68 (3) (1987) 295–307.
- [5] Y. Sivathanu, G. Faeth, Generalized state relationships for scalar properties in nonpremixed hydrocarbon/air flames, *Combustion and Flame* 82 (2) (1990) 211–230.
- [6] S. Fischer, B. Hardouin-Duparc, W. Grosshandler, The structure and radiation of an ethanol pool fire, *Combustion and Flame* 70 (3) (1987) 291–306.
- [7] A. Hamins, A. Lock, The Structure of a Moderate-Scale Methanol Pool Fire, NIST Technical Note 1928, National Institute of Standards and Technology (2016).
- [8] S. Kim, K. Lee, A. Hamins, Energy balance in medium-scale methanol, ethanol, and acetone pool fires, *Fire Safety Journal* 107 (2019) 44–53.
- [9] E. Weckman, A. Strong, Experimental investigation of the turbulence structure of medium-scale methanol pool fires, *Combustion and Flame* 105 (1) (1996) 245–266.
- [10] A. Hamins, S. Fischer, T. Kashiwagi, M. Klassen, J. Gore, Heat feedback to the fuel surface in pool fires, *Combustion Science and Technology* 97 (1-3) (1993) 37–62.
- [11] A. Hamins, M. Klassen, J. Gore, T. Kashiwagi, Estimate of flame radiance via a single location measurement in liquid pool fires, *Combustion and Flame* 86 (3) (1991) 223–228.
- [12] A. Hamins, T. Kashiwagi, R. R. Buch, Characteristics of pool fire burning, in: *Fire Resistance of Industrial Fluids*, ASTM International, 1996.
- [13] A. Lock, M. Bundy, E. Johnsson, A. Hamins, G. Ko, C. Hwang, P. Fuss, R. Harris, Experimental Study of the Effects of Fuel Type, Fuel Distribution, and Vent Size on Full-Scale Underventilated Compartment Fires in an ISO 9705 Room, NIST Technical Note 1603, National Institute of Standards and Technology (2008).
- [14] A. Hamins, K. Konishi, P. Borthwick, T. Kashiwagi, A comparative study of n-propanol, propanal, acetone, and propane combustion in laminar flames, *Proceedings of the Combustion Institute* 26 (1) (1996) 1429–1436.
- [15] Z. Wang, W. Tam, K. Lee, J. Chen, A. Hamins, Thin filament pyrometry field measurements in a medium-scale pool fire, *Fire Technology* (September 2019).
- [16] C. Shaddix, Correcting thermocouple measurements for radiation loss: a critical review, Tech. Rep. CONF-990805, Sandia National Laboratories (1999).
- [17] M. Choi, G. Mulholland, A. Hamins, T. Kashiwagi, Comparisons of the soot volume fraction using gravimetric and light extinction techniques, *Combustion and Flame* 102 (1-2) (1995) 161–169.
- [18] G. H. Ko, A. Hamins, M. Bundy, E. L. Johnsson, S. C. Kim, D. B. Lenhart, Mixture fraction analysis of combustion products in the upper layer of reduced-scale compartment fires, *Combustion and Flame* 156 (2) (2009) 467–476.
- [19] R. Falkenstein-Smith, K. Sung, J. Chen, A. Hamins, The Structure of Medium-Scale Pool Fires, NIST Technical Note in Review, National Institute of Standards and Technology (2019).
- [20] G. Heskestad, Luminous heights of turbulent diffusion flames, *Fire Safety Journal* 5 (2) (1983) 103–108.
- [21] Ü. Ö. Köylü, G. M. Faeth, Carbon monoxide and soot emissions from liquid-fueled buoyant turbulent diffusion flames, *Combustion and Flame* 87 (1) (1991) 61–76.